*Article*

# Experimental Study on the Effect of Hull Deformation on the Relative Attitude between Shaft and Bearing

**Weixin Zhou** [1,2], **Yao Zhao** [1,2], **Hua Yuan** [1,2,*] **and Zhaoxin Ren** [1,2]

1   School of Naval Architecture and Ocean Engineering, Huazhong University of Science and Technology, Wuhan 430074, China
2   Hubei Key Laboratory of Naval Architecture and Ocean Engineering Hydrodynamics (HUST), Wuhan 430074, China
*   Correspondence: yuanhua@hust.edu.cn; Tel.: +86-138-7122-9756

**Abstract:** The unclear change laws of bearing offset and rotation, both of which influence the condition of shaft alignment during hull deformation, make it difficult to optimize shafting design. In this paper, an integrated hull-bearing-shaft model is designed and built for a cantilever beam loading test. Displacement sensors are utilized to determine the change in displacement of the hull, bearings, and shaft. The pressure distribution at the bow and stern ends of the bearing is measured using a new type of thin-film pressure sensor. The test results show that the rotation angle of the shaft and bearing varied differentially during hull deformation, and the magnitude of the shaft-bearing angle was comparable to the rotation angle. The measured rotation angles of the front and rear ends of the stern tube bearings are opposite to the theoretical value of a cantilever beam, indicating that the stern tube has a non-negligible effect on local deformation, and it is recommended to measure the bearings directly as opposed to the alternative structure to obtain the rotation. The change pattern of the shaft and bearing attitude does not change with the different initial state of the shaft, which indicates that the initial error of installation will be retained during the hull deformation process. The change pattern of the shaft and bearing attitude is unaffected by the initial state of the shaft, indicating that the initial installation error will persist during hull deformation. In some instances, the bearing reaction force remained unchanged, but the shaft-bearing angle and bearing pressure altered, indicating that the bearing condition cannot be determined solely by the bearing reaction force. The results of bearing pressure and the shaft-bearing angle can be compared, indicating that the thin-film pressure sensor can be used to determine the status of the shaft-bearing angle, particularly during the installation phase.

**Keywords:** hull deformation; shaft alignment; cantilever model tests; bearing offset; rotation angle; bearing pressure

## 1. Introduction

The propulsion shaft system is the ship's power source, and its operational condition has a significant impact on safety and economy [1,2]. The optimal working condition of a propulsion shaft system is the design stage, also known as the rational alignment state, in which multiple bearings are loaded to a reasonable value and rotated to match shaft deflection [3–5]. Despite the fact that the propulsion shaft system can be adjusted to the rational alignment state using a variety of methods during the installation process, the working state will change and deviate from the design state during the ship's launching and voyage due to the hull deformation caused by the variation of internal and external loads [6]. Improper shaft alignment causes improper bearing reactions, which can result in a variety of shaft failures, including excessive vibrations, seal leaks, excessive wear, engine overload, temperature increases, and abnormal noise [7–9].

Bearings are the primary components that connect the hull structure to the shaft system. The condition of the shaft alignment is determined by the position and attitude of

the bearings [10]. The key to analyzing the effect of ship deformation on shaft alignment is to determine the bearings' offset and rotation. Zhou [11] pointed out that the bearing offset influences the bearing reaction force, and the bearing rotation angle influences the distribution of bearing pressure. In the current state of the art, the rotation of the bearings is frequently ignored, and the influence of bearing offset on shaft alignment is given more consideration.

Acquisition of bearing offset data can be accomplished in three distinct ways: the measurement method, the finite element method (FEM), and the beam theory calculation method. One can divide measurement techniques into laser techniques and strain techniques. In shipyards, one of the procedures for shaft installation is bearing centering, which is performed by installing laser equipment at the last bearing and shining it forward to determine the offset of the individual bearings, which is then adjusted accordingly. This technique is only applicable when the shaft has not yet been installed. Using a laser device to measure the offset of the structure near the bearing instead of the bearing itself and calculating the change in bearing reaction force accordingly, some researchers [12,13] have circumvented the problem of being unable to measure the shaft when it is installed. Lee [12] then developed a finite element model of the shaft system in order to analyze the contact pressure within the bearing. However, laser measurements do not capture the rotation of the bearings, so the bearing pressure analysis is inaccurate. Cheng [14] has created a new measurement device that employs eddy current sensors to monitor shaft alignment and laser sensors to measure ship deformation. The device's effectiveness has been validated under laboratory conditions. This device has also been utilized for measuring the alignment of fan bearings [15]. However, difficulties remain in applying the device to measurements on actual ships, as the shaft system is lengthy and multiple bearings are arranged in separate compartments, obstructing the optical path. In addition, the substitution of bearing offsets with nearby measuring structures has unknown effects.

Strain measurement is yet another indirect method for measuring bearing offset. The principle is to theoretically calculate the influence coefficient of each bearing offset on the shaft's bending moment, then install strain gauges on the shaft to measure the change in the shaft's bending moment under different operating conditions, and finally invert the bearing offset [1,16–19]. Adopting the wireless transmission device can alleviate the difficulty of data collection when the shaft is rotating. When calculating the influence coefficient, the method simplifies both the shaft and the bearing, resulting in a discrepancy between the calculated influence coefficient and the actual situation. Additionally, the initial state cannot be measured because this is an incremental measurement procedure. In addition, wireless transmissions cannot be monitored for an extended period of time due to the duration of battery power.

Direct measurement of bearing offset remains difficult to implement, and numerous researchers have attempted to obtain bearing offset during hull deformation using FEM [20,21]. FEM has the advantage of requiring only a computer, making it much simpler to implement than measurements. Generally, if the FEM model is more accurate and the mesh is finer, the results will be closer to the actual outcomes. Shi [22] created an FEM model of a 76,000 DWT product oil tanker in order to calculate bearing offsets under various wave and temperature conditions. Murawski [23] constructed a 2000 TEU container stern model that included the propulsion system. Using the model, he analyzed the impact of hull deformation on bearing offset at various phases of construction. Seo [24] analyzed the deformation of a 300,000 DWT very large crude oil carrier under various drafts and the effect on shaft alignment using FEM. He discovered that the main engine compartment's deformation follows an opposite pattern to that of the whole ship. Zhang [25] used AQWA to calculate the wave load per unit wave height at various frequencies in order to acquire the wave pressure distribution when calculating the effect of hull deformation on the support force of the shaft, resulting in a more accurate hull deformation.

Although FEM is capable of simultaneously obtaining the bearing offset and rotation, the researchers only considered the bearing offset and its influence on the bearing reaction

force, ignoring the bearing rotation's impact on the bearing pressure. Additionally, there are some issues with FEM. First, the structure and arrangement of the entire ship are intricate, and the workload associated with building the entire model is not minor. Second, the mesh quality requirement of FEM necessitates the simplification of numerous structures, making it difficult to assess the bearing offset. For instance, the main engine is simplified as a mass point in the structural model, which significantly alters the local deformation of the bottom and the offset and rotation of the bearings compared to the actual situation.

The theoretical calculation technique has been utilized in far fewer studies than the other two methods. This is due to the complexity of the hull structure, which necessitates excessive simplification for the calculation to be implemented, but it will undoubtedly result in a large error in the results. Low [26] assumed that the position of the outer bearing of the hull was a straight line and that the position of the inner bearing was equal to the hull deflection value. This method only considers the global deformation of the hull. Zhou [11] divided the hull deformation influencing the shaft alignment into global and local deformations and calculated the local deformation of the bearings using the grillage beam model. However, these methodologies have not been validated by comparing them with actual ship tests.

Some researchers [27–31] have examined the influence of hull deformation on shaft alignment by constructing an experimental shaft system rig in the laboratory or by mathematically calculating a shaft. The focus of these studies is the distribution of pressure inside the bearing, and the results indicate that the bearing rotation angle has a significant impact on the pressure distribution. In these experiments, however, the bearing's offset and rotation are active inputs. It is challenging to ascertain if these values correspond to the actual situation during hull deformation. Furthermore, the displacement and rotation of the bearing are the result of hull deformation, and it is challenging to determine the deformation law of the bearing and shaft under hull deformation using the above tests. In addition, it is uncertain whether the initial state of the bearings and shafts influences the alignment state of the shafts when the hull is deformed differently.

The contribution of this paper is the design and construction of an integrated hull-bearing-shaft model for cantilever loading testing in the laboratory. Changes in the displacements of the hull, bearing, and shaft are measured simultaneously. The test data are used to visually analyze the change rule for the position and rotation angle of the shaft and bearing under hull deformation. The change rule is useful for providing design guidance for the shaft system. Meanwhile, a new form of thin-film pressure sensor is employed to measure the pressure distribution at the bearing's end. By using the pressure distribution to reflect the shaft-to-bearing angle, the subjective error introduced by the feeler gauge can be avoided. This is of great significance for improving measurement accuracy and enhancing the shaft system installation procedure.

The structure of the paper is as follows: the first section examines the research on the impact of hull deformation on shaft alignment. The second section explains the test's design. The third section describes the test's measurement instruments and measurement conditions. In the fourth section, test results and analyses are presented. The fifth section summarizes the research.

## 2. Schematic Design of the Test

Numerous academics have acknowledged the impact of hull deformation on shaft alignment. However, intuitive measurement data of shaft and bearing position and attitude with hull deformation are extremely limited, and their change rule cannot be analyzed. The lack of measurements on the actual ship is due to the vessel scale being too large. It is impossible to deform the large ship continuously with stable continuous loading. In addition, the shaft arrangement of the actual ship traverses multiple compartments, which makes the measurement range too large and the arrangement of measurement instruments challenging. A scaled-down hull-bearing-shaft model was created and used in a laboratory

cantilever loading test to collect data on the position and attitude of the shaft and bearing as the hull deforms.

### 2.1. General Plan of the Test

The hull deformation that affects the shaft alignment can be categorized into three situations. In the first scenario, the hull is in a dry dock during construction. At this time, the installation of equipment and other structures will alter the ship's weight distribution, resulting in hull deformation. Second, as the hull is progressively submerged in the water during the launching phase, water pressure causes deformation. Thirdly, hull deformation is caused by the fluctuating load and waves during the voyage, and the deformation amplitude is also continuously changing.

Rigid body displacement and elastic deformation displacement are present in all three situations of hull deformation. The effect of rigid body displacement on shaft alignment is negligible, and it is not necessary to account for it in the testing procedure. Elastic deformation displacement refers to the global and local deformation resulting from changes in internal and external loads in the hull coordinate system [11]. Global deformation typically refers to the flexural deformation of the hull as an elongated thin-walled beam, whereas local deformation is the deformation of the local structure near the bearing as a result of the change in local pressure on the plate. Global deformation is the primary focus of this paper.

The primary focus of this paper is global deformation. The key to achieving global deformation is deflecting the hull. For the construction phase, the weight of the apparatus installation can be viewed as a concentrated force, and the deformation at this time resembles that of a cantilever beam. During the launching and sailing phases, the deformation is more complicated and comprises an infinite number of deformation forms. Although the sailing state corresponds to the majority of the ship's life cycle, the use of cantilever beams to achieve hull deflection can show the effect of hull deformation on shaft alignment, especially on the initial error.

Figure 1 depicts the overall test design; the test model resembles a cantilever beam with the front end fixed rigidly to a shear wall and the rear end loaded by a hydraulic cylinder to induce flexural deformation. When designing the prototype vessel, only the ship's stern was considered. This is because the propulsion shaft system is also predominantly located at the aft end, and the hull's aft structure has a greater effect on the shaft system. The test model has a shaft supported by three bearings; the front end of the shaft simulates the restraining effect of coupling by limiting vertical and longitudinal displacements; and a weight is suspended from the rear end of the shaft to simulate the propeller's counterweight.
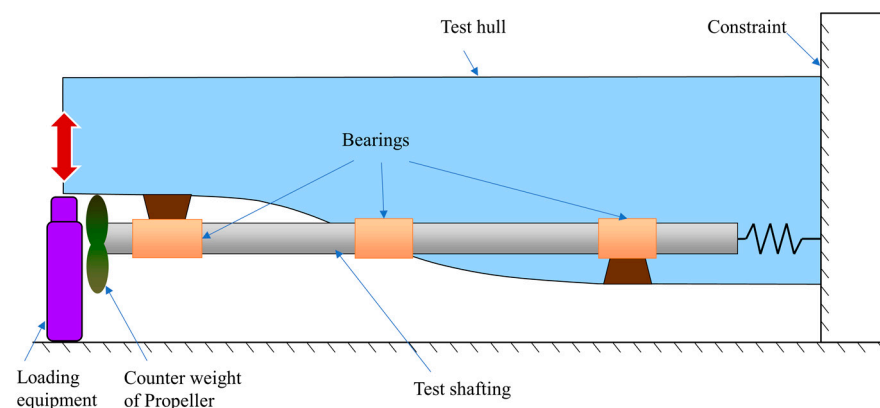


**Figure 1.** Schematic diagram of the overall test plan.

Bearing offsets influence bearing reaction forces but do not reflect variations in bearing pressure. Both bearing offsets and shaft-to-bearing angles influence alterations in bearing pressure. The bearing position and shaft-to-bearing angle are the most important quantities

to reflect the condition of shaft alignment, and both are determined by the hull-bearing-shaft mechanism's spatial position. Therefore, the primary monitoring quantities in this test procedure are the displacement of bearing and shaft.

During this test, the loading was quasi-static, meaning that each time the loading force attained a certain value and stabilized for a certain time, the hull deformation and bearing pressure were measured. The quasi-static process was used to simulate the continuous deformation of the ship's hull and to track the trend of the critical quantities throughout the process. The deformation of the hull by gravity and wave force is much greater than the deformation caused by the rotation of the shaft, so the quasi-static process is able to reflect the relationship between the hull, bearing, and shaft position change during the deformation of the actual ship, even though the entire shaft system is not rotated.

### 2.2. Design of Test Model

The advantage of conducting the hull-bearing-shaft deformation measurement experiments in the laboratory is that both loading and measurement are simpler to implement. However, there are some issues with the test model's design. In ship testing, a scaled-down model is typically used to represent the larger model's characteristics. Table 1 displays the scale of the test hull in accordance with the full similarity theory, based on the loading conditions and spatial extent of the laboratory, after selecting a scale ratio of 1/5. It can be seen that the corresponding plate thickness is 1.6 mm; however, the builder specified that welding a 1.6 mm thick plate results in severe welding distortion. The initial construction error introduced by welding distortion will have a significant impact on the test results, resulting in an inability to analyze the hull deformation's composition. There are currently scaling hypotheses that propose a different scaling ratio for thickness. However, this creates a new issue, which is that the test hull's rigidity is excessively high. According to the builder's recommendations, it is relatively simple to control weld distortion on hulls with weld thicknesses greater than 5 mm. Calculations indicate that a loaded force of 240 t is required to produce a maximum deformation of 10 mm for a test hull with a plate thickness of 5 mm and dimensions identical to Table 1. This causes significant loading difficulties in the laboratory. The excessive internal longitudinal and transverse bulkheads are the primary cause of the scaled-down model's high stiffness, as similar models necessitate the retention of these bulkheads. Using the scaled model approach to design the model would necessitate finding a new scaling theory to simplify the model in order to satisfy the constraints of regulating the weld deformation and the loading force not exceeding the laboratory's loading capacity.

**Table 1.** Parameters of original ship and scaled-down model using full similarity theory.

|  | Original Ship | Scaled-Down Model |
|---|---|---|
| Length of stern | ~40.0 (m) | 8.0 (m) |
| Breadth | 12.0 (m) | 2.4 (m) |
| Height | 10.0 (m) | 2.0 (m) |
| Plate thickness | ~8 (mm) [1] | 1.6 (mm) |

[1] Plate thicknesses varied at various locations within the hull structure; here, the plate thicknesses are averaged across the main structure.

Considering that the purpose of this study is not to use a scaled-down model to invert the position relationship between the hull and the shaft of the original ship during hull deformation, rather, it is intended to demonstrate the importance of paying close attention to the relative inclination change of the shaft and bearing during hull deformation. Maintaining the relative relationship between the flexural deformation of the hull girder and the flexural deformation of the shaft system is therefore the primary concern in the design of the model. Consequently, the deflection theory is not utilized in the design of the model, but the following principles are followed: First, the ratio of the cross-sectional moment of inertia of the test hull to the moment of inertia of its shaft is comparable to that

of the original ship, with values of $2.79 \times 10^3$ and $2.59 \times 10^3$ for the designed test hull and the original ship, respectively. Second, the bearing arrangement should include as many different forms of the original ship as possible, such as outboard bearings, inboard bearings, and stern tube bearings. The different forms of bearings in the vicinity of the hull structure may also affect the change rule for the angle of change of the shaft and bearings. Finally, the size design complies with the design and construction specifications of the China Classification Society (CCS), so that the design of the structure itself is a small ship's stern structure that can directly reflect the same scale conditions of the hull deformation on the shaft-bearing angle of influence. Figure 2 depicts the test model's final configuration.
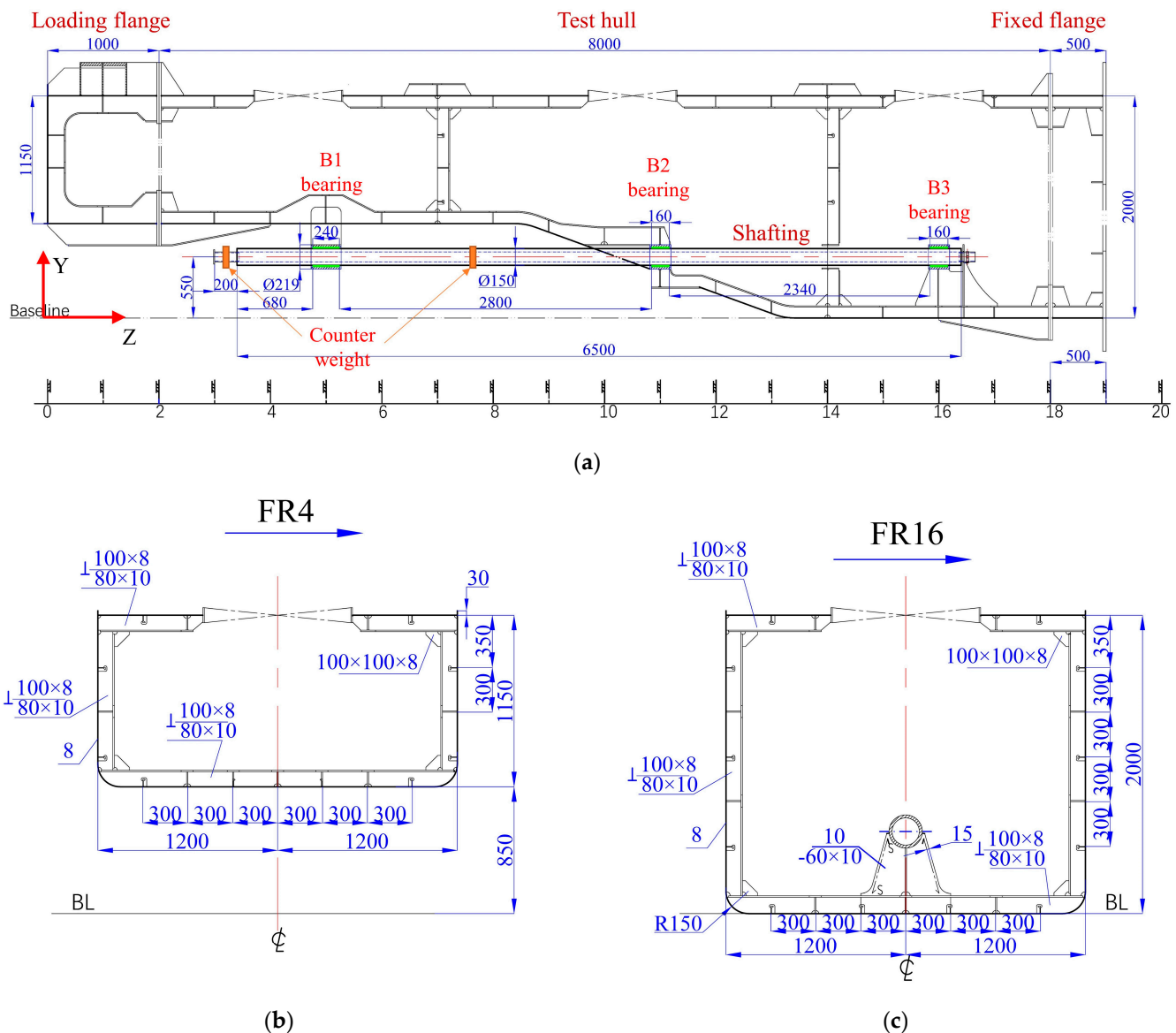


**Figure 2.** Design drawings of the test model. (**a**) Center-longitudinal section; (**b**) Cross-section of FR4; (**c**) Cross-section of FR16.

The test model consists of the test hull and the shaft system. The test hull has a single bottom and longitudinal skeleton; the interior is divided into three compartments by two transverse bulkheads; and there are three openings on the deck for entering and exiting, as depicted in Figure 2a. The test's solitary shaft is located in the middle of the ship's keel and has a length of 6.5 m. The shaft is supported by three bearings, B1, B2, and B3, each of which is located in a separate compartment. The B1 bearing is located on the exterior side

of the last compartment of the hull and is secured by an external bracket; the B2 bearing is located in the middle compartment and is the stern tube bearing; and the B3 bearing is located in the front compartment, which is on the interior side of the hull. Tables 2 and 3 outline the primary characteristics of the three bearings and the test hull. Figure 2b,c are cross-sectional views of rib positions 4 and 16, respectively. The numbers marked with an inverted T in the figures represent the cross-sectional dimensions of the T profiles, and the numbers marked with a "-" represent the dimensions of the flats. Dimension markings in the drawing are in millimeters.

**Table 2.** Table of bearing parameters.

| Parameter | Number | Parameter | Number |
|---|---|---|---|
| Material | Thordon | Thickness | 25 (mm) |
| Elastic modulus | 605 (MPa) | Poisson's ratio | 0.45 |
| Length-diameter ratio of B1 | 1.6 | Length-diameter ratio of B2 and B3 | 1.07 |

The front and fixed flange and rear loading flange are installed on the test hull to shield it from damage during the test. The test model includes flanges measuring a total of 9.5 m in length, 2.4 m in breadth, and a maximum of 2.0 m in height. The length direction is denoted by Z, with the fixed flanges as the positive direction; the height direction is denoted by Y, with the top as the positive direction; and the width direction is denoted by X, with the port side as the positive direction. The actual test hull after construction is shown in Figure 3.



**Figure 3.** Physical drawing of hull structure.

**Table 3.** Table of parameters of the test hull.

| Parameter | Number | Parameter | Number |
|---|---|---|---|
| Material | AH32 | Length | 8.0 (m) |
| Elastic modulus | 210 (GPa) | Breadth | 2.4 (m) |
| Poisson's ratio | 0.3 | Height | 2.0 (m) |
| Thickness of plate | 8 (mm) | Frame space | 500 (mm) |

*2.3. Special Handling of Shafting Installation*

The procedure of installing a shaft consists of four stages: shaft system illumination and centering; bearing seat boring; bearing installation; and shaft installation [1]. During the installation, the temperature must be rigorously regulated to prevent the hull from deforming and affecting the position of the bearings. However, the installation is conducted in the dry dock, and the relative attitude of the shaft and bearings must satisfy the design specifications at this time. When the ship is transferred from the dry dock to the water, the buoyancy force deforms the hull, and the relative attitude becomes unknown.

In this test, the same problem was encountered. If the bearings are bored and the shafts are installed first, the hull will also endure some deformation during transport and model installation, which is difficult to monitor and will render the initial state of the test unknown. In order to obtain an accurate initial state, the bearing boring and shaft installation processes were arranged after the test model was fixed on the shear wall. The mounting fixation state of the test model on the shear wall (subject to gravity only) is the initial state of the test, and the axis line of bearings after boring is straight. Thus, when subsequently analyzing the initial condition of the bearing and the shaft, the initial bearing offset can be determined to be 0 mm, and the initial shaft deflection curve can be calculated accordingly. Figure 4 depicts the bearing boring operation in which the test model has been attached to the shear wall and leveled in the transverse direction.



**Figure 4.** On-site boring picture after the test hull installation.

The bearing bush is affixed using the same cold shrinkage method as the vessel's installation procedure. The bearings are shrunk by cooling them with liquid nitrogen, and then they are deposited in the holder to expand at room temperature. Figure 5a depicts the three bearings without mounting, and Figure 5b depicts the chilled bearings.
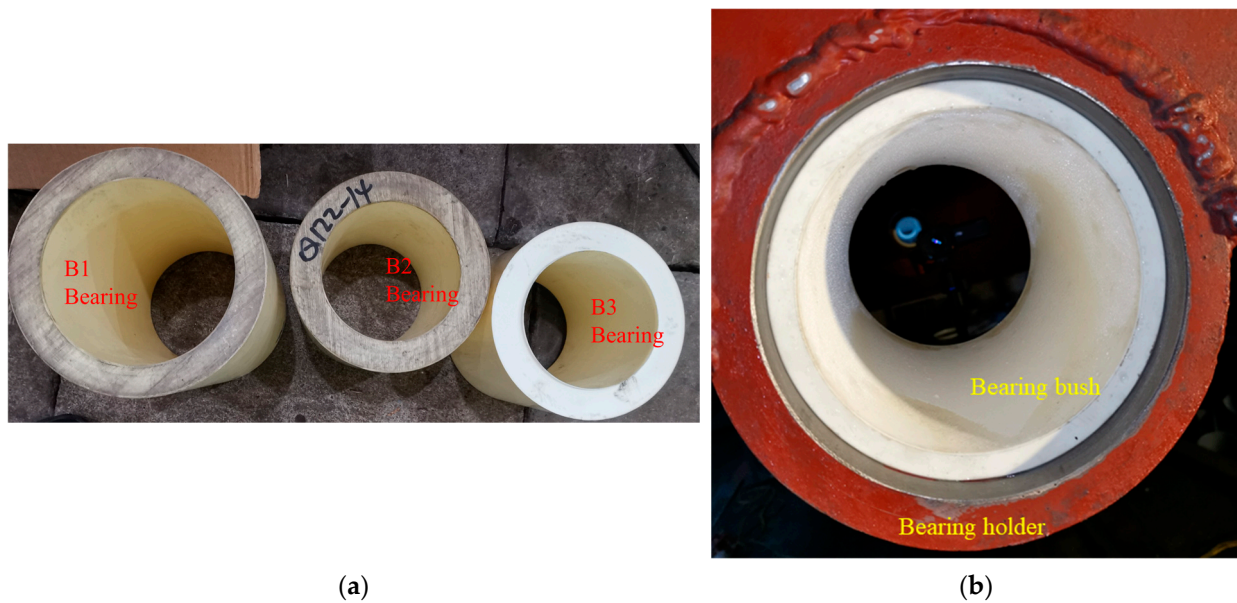
**Figure 5.** Thordon bearings. (**a**) Bearings without mounting; (**b**) chilled bearing.

## 3. The Measurement Systems

Changes in the relative positional state between the hull, bearing, and shaft produce the effects of hull deformation on the shaft system. The bearing offset will cause each bearing reaction force to change proportionally, and the change in shaft-to-bearing angle will cause the bearing pressure to change. In this test, two sets of measurement systems were set up to record the changes in key parameters during the process of hull deformation. These systems are the displacement measurement system and the bearing pressure measurement system.

### 3.1. The Displacement Measurement System

During the test, the measurement of deformation displacement was divided into two sections. The first component is the bearings; at the front and rear ends of the three bearings B1, B2, and B3, displacement gauges are positioned to measure vertical displacements (y-direction). The second component is the shaft, and along the shaft's longitudinal axis, the displacement gauges are arranged at the shaft's bottom. Due to the minor displacements near the fixed end, no additional measurement points were added to the shaft inside the cabin. Figure 6 depicts the displacement gauge measurement sites for the bearing and shaft. Table 4 outlines all of the displacement gauge's numbers.
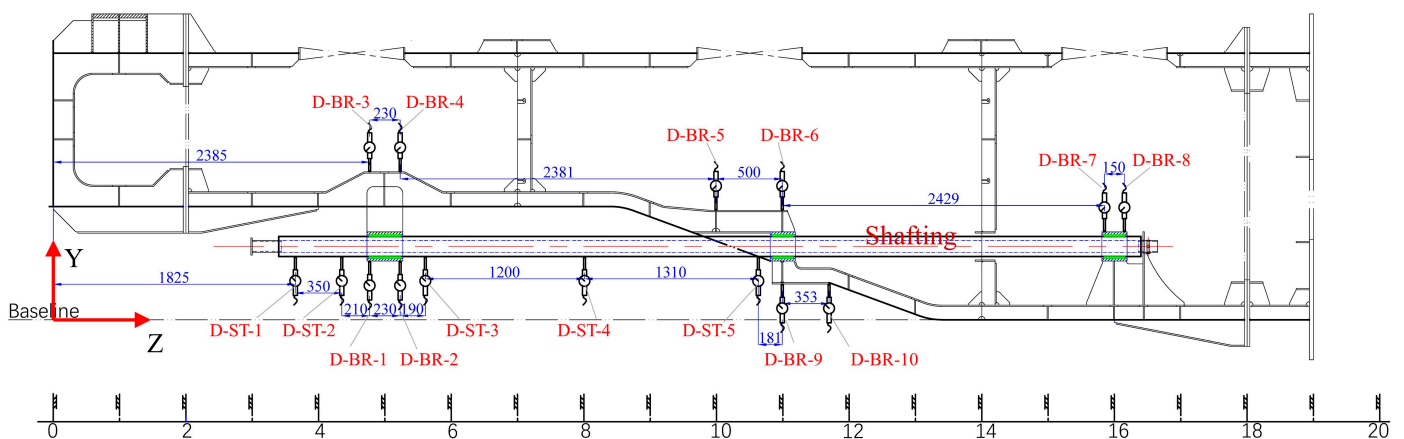


**Figure 6.** Schematic diagram of the measurement position.

**Table 4.** Table of displacement gauge numbering.

| Measured Object | NO. | Quantity |
|---|---|---|
| Bearing B1 | D-BR-1,2,3,4 | 4 |
| Bearing B2 | D-BR-5,6,9,10 | 4 |
| Bearing B3 | D-BR-7,8 | 2 |
| Shaft | D-ST-1,2,3,4,5 | 5 |

Donghua Testing (DONGHUA) Company's 5 G103 linear displacement gauge was used as the test's displacement gauge. The 5G103 is a resistive displacement gauge that has a long life, good linearity, good repeatability, a simple structure, is user-friendly, and is less susceptible to environmental factors. The gauge is shown in Figure 7a, and its parameters are listed in Table 5. As depicted in Figure 7b, the data acquisition instrument is a Donghua DH3816N strain box.



(a)                                            (b)
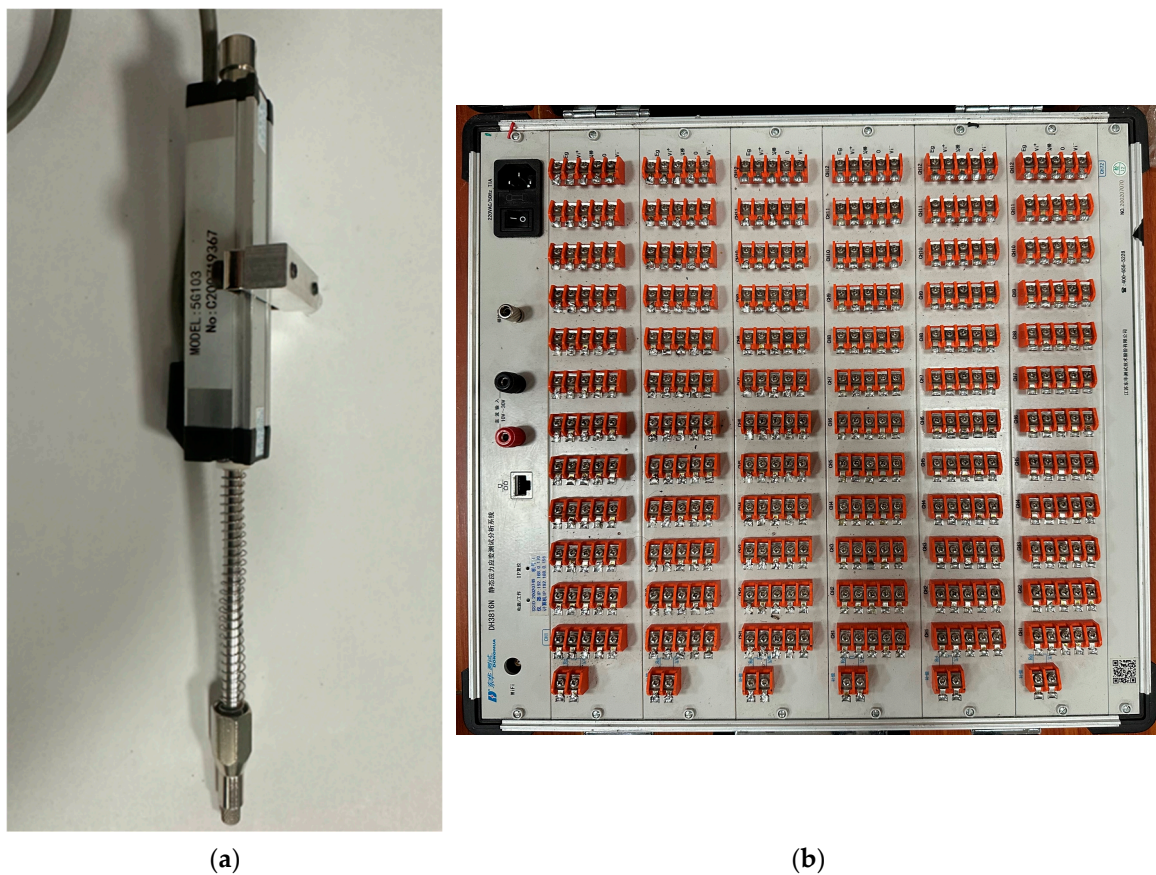
**Figure 7.** Diagram of displacement measurement equipment. (**a**) Displacement gauge; (**b**) data acquisition instrument DH3816N.

**Table 5.** Parameters of displacement gauge.

| Parameter | Number | Parameter | Number |
|---|---|---|---|
| Type | 5G103 | Maximum working speed (m/s) | 5 |
| Range (mm) | 50 | Repeatability errors (mm) | 0.005 |
| linear accuracy (%FS) | ≤0.25% | Working temperature (°C) | −20~+80 |
| overall dimension (mm) | 115 × 14.8 × 25 | | |

To ensure that the measured displacements are absolute values in the geodetic coordinate system, all displacement instruments were fitted with geodetic coordinate system-appropriate fixtures. As depicted in Figure 8, the displacement gauges of the shaft are

mounted on a truss structure that is directly fixed to the ground. The truss structure extends from the opening at the top of the test vessel into the cabin to provide a mounting platform for the in-cabin displacement gauges that are suspended inverted from bearings B1, B2, and B3. Due to the fact that the stiffness of the displacement gauge is approximately 0.1 N/mm, which is significantly less than the stiffness of the truss structure, which is approximately 400 N/mm, the influence of the truss structure on the displacement results can be disregarded.
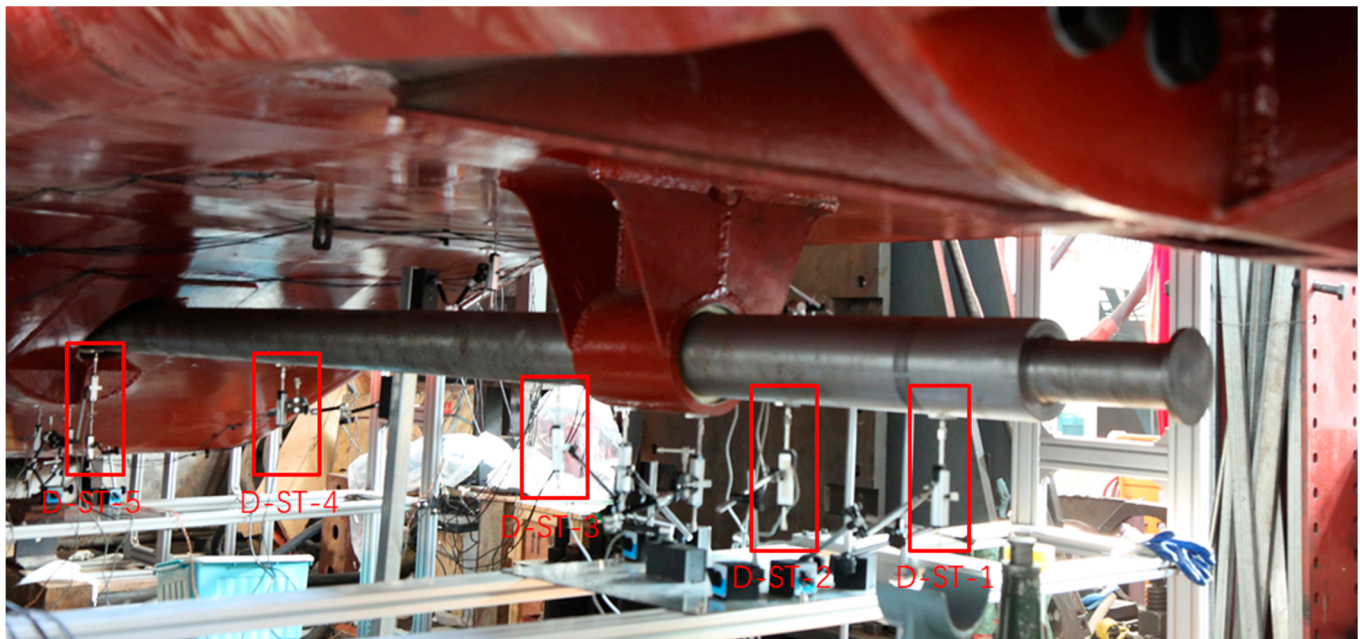


**Figure 8.** Shaft displacement gauge installation diagram.

### 3.2. Bearing Pressure Measurement Systems

Bearing pressure is separated into two categories. The first is the contact pressure when the shaft is either not rotating or moving at a slow speed. The second is the hydrodynamic pressure at a particular rotational speed. The relative attitude of the shaft and bearing has an effect on the distribution of both pressures. This test primarily measures contact pressure.

As depicted in Figure 9, a thin-film pressure gauge is utilized to measure the pressure. The thin-film gauge is a resistive sensor whose primary material is a piezoresistive thin-film material, which corresponds to the figure's "Sensor" label. When pressure is applied, the resistance of the piezoresistive nanolayer contained within the gauge varies due to particle deflection. By measuring the change in resistance, it is possible to measure the change in surface pressure. The sensor is connected to the acquisition device via signal wires and joints. However, a thin-film pressure gauge can only output a single value, so the measurement is the average force on the entire surface of the pressure plate. Table 6 displays the parameters of the pressure gauge.

**Table 6.** Parameters of the thin-film pressure gauge.

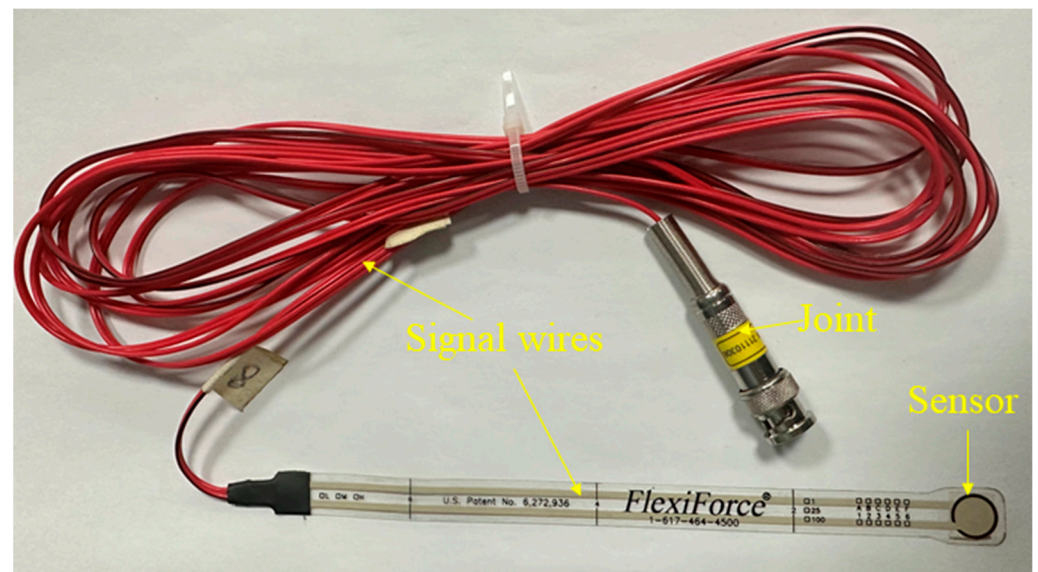| Parameter | Number | Parameter | Number |
|---|---|---|---|
| Type | LC-201-8-5 | Range (N) | 660 |
| Thickness (mm) | 0.2 | Diameter of Sensor (mm) | 9.52 |
| Working temperature (°C) | −9~60 | Linearity | 99% |
| Linearity error | <±3% | Repeatability | <±2.5% |

**Figure 9.** Physical drawing of the thin-film pressure gauge.

Shanghai Yicheng Test Equipment Co., Ltd. (Shanghai, China) provided the thin-film pressure gauge. As shown in Figure 10, the thin-film pressure gauge, the acquisition device MFF-8, the process software, and the force calibration instrument comprise the bearing pressure measurement system [32]. As the resistance value of the thin-film pressure gauge is highly influenced by temperature, it is necessary to calibrate the gauge with a force calibration instrument and adjust the temperature deviation parameter in the software prior to the start of each measurement.
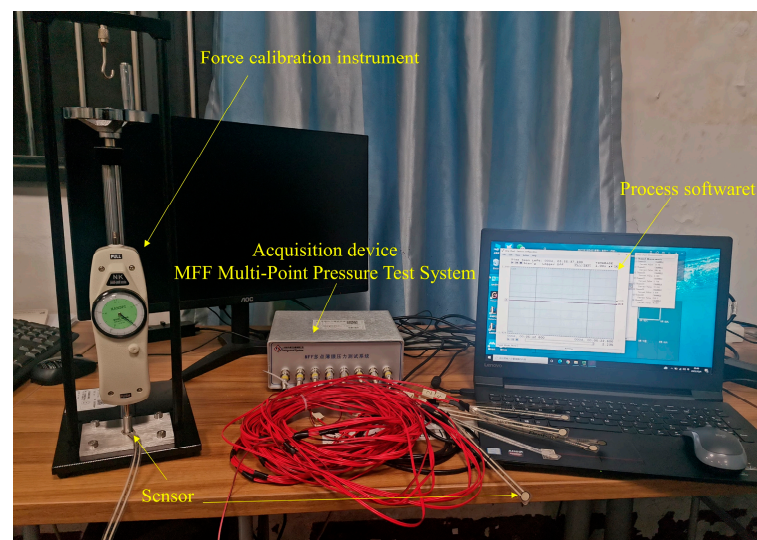


**Figure 10.** Pressure measurement systems.

Conformal contact exists between the shaft and bearing, meaning that the outer diameter of the shaft is near the inner diameter of the bearing. Even though the thin-film pressure sensor is already quite thin, the insertion of a pressure gauge impacts the accurate distribution of internal pressure. The purpose of this pressure measurement is not to obtain an exact contact pressure value but rather to determine, using relative pressure values, whether the shaft-to-bearing angle has changed during hull deformation.

As shown in Figure 11a, the pressure gauges which are indicated by a red circle in the figure are primarily located at the front and rear ends of the bearings. P-B1-2 and 3 are positioned at the front end of the B1 bearing, 20 mm from the end face and $\pm 20°$

from the bottom along the circumferential direction. P-B1-1 and 4 are situated at a 10° circumferential angle away from the base relative to P-B1-2, and 3, respectively. P-B1-5, 6, 7, and 8 are located at the rear end of the B1 bearing; they correspond in circumferential orientation with P-B1-1, 2, 3, and 4. Figure 11b depicts the pressure gauge installation. Marking the line on the shaft in advance guarantees the correct installation location of the instruments. Due to the limited range of the pressure sensors, if they are arranged in the bottom contact area, the measurement may begin to exceed the range, and no changes in data can be detected. Therefore, the eight pressure sensors were divided into two groups, one for the measurement group and one for the control group. They were situated inside and outside the contact boundary, with the measurement group P-B1-2,3,6,7 inside the contact area and the control group P-B1-1,4,5,8 outside the measurement area.
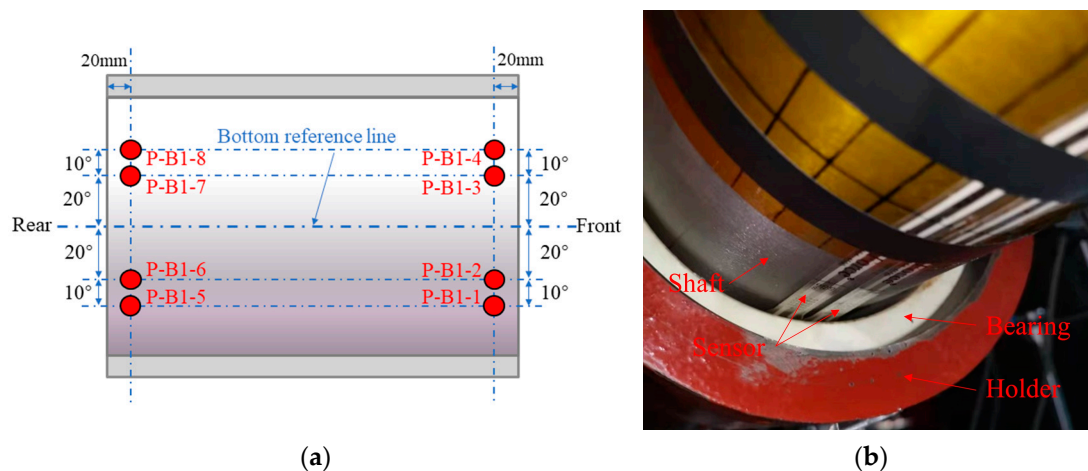


(**a**)　　　　　　　　　　　　　　　　　　　　　(**b**)

**Figure 11.** Arrangement of the thin-film pressure gauge. (**a**) Schematic layout; (**b**) installation diagram.

*3.3. Test Conditions*

As shown in Table 7, four working conditions were set for this test. In conditions 1 and 2, the counterweight at the aft end of the shaft is 100 kg, the suspension position is 100 mm from the end of the shaft, and the negative sign indicates the position near the stern of the hull. The maximal loading force for condition 1 is "+30 t", where the positive sign indicates upward loading. For condition 2, the utmost downward load is 20 t, and for conditions 3 and 4, the shaft counterweight remains at 100 kg, but its position is moved to 2.1 m from the shaft's end. In Figure 2a, the counterweight locations are indicated by yellow squares.

**Table 7.** Table of test conditions.

| Condition Number | Working Condition | Maximum Loading Force | Repetition Number |
|---|---|---|---|
| 1 | Counterweight 100 kg at −100 mm | +30 t | 3 |
| 2 | Counterweight 100 kg at −100 mm | −20 t | 3 |
| 3 | Counterweight 100 kg at 2100 mm | +30 t | 3 |
| 4 | Counterweight 100 kg at 2100 mm | −20 t | 3 |

"+" indicates the vertical load direction is upward; "−" indicates the vertical load direction is downward.

## 4. Test Results and Discussion

*4.1. Displacement Results*

As shown in Figure 12, the results of the D-BR-3 and D-ST-1 displacement gauges were selected for comparison following the measurement of various working conditions. Multiple measurements yield consistent results, as is evident. The D-ST-1-gauge results for condition 2 differ the most, with a maximum error of 3% at the maximum load. The displacement curve rises as the load increases, and its overall trend is linear. This indicates that the test hull deformation is within the elastic range. In addition, the results of D-ST-1 are always slightly larger than those of D-BR-3, which is due to the fact that the test hull is

subjected to a similar force as a cantilever beam during the test. The further away from the fixed end, the larger the displacement value. It is easy to see from Figure 6 that the D-ST-1 is further from the fixed end. The results of the remaining displacement gauges follow the same pattern as shown in Figure 12, with the exception of a few numerical differences that will not be displayed again.
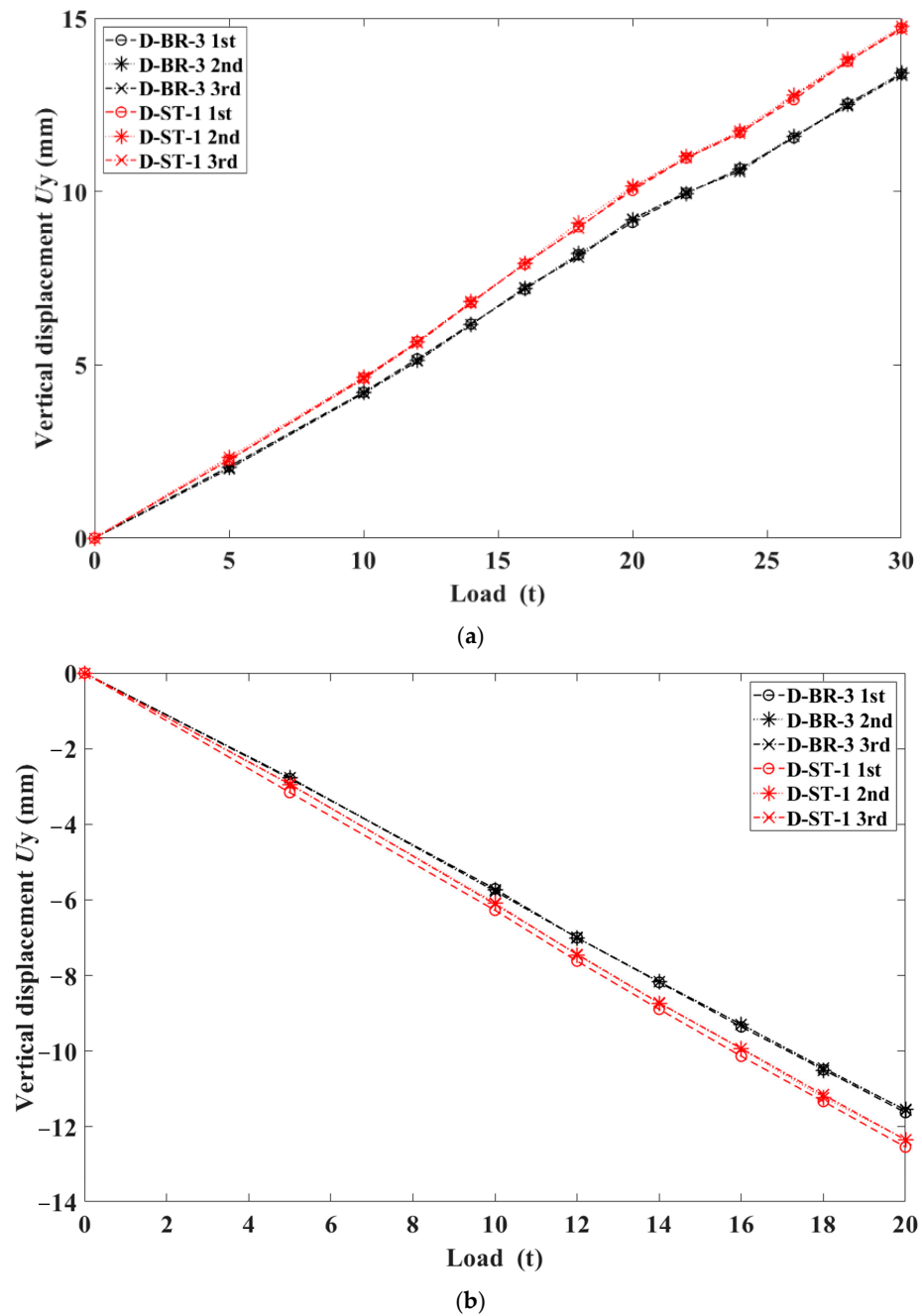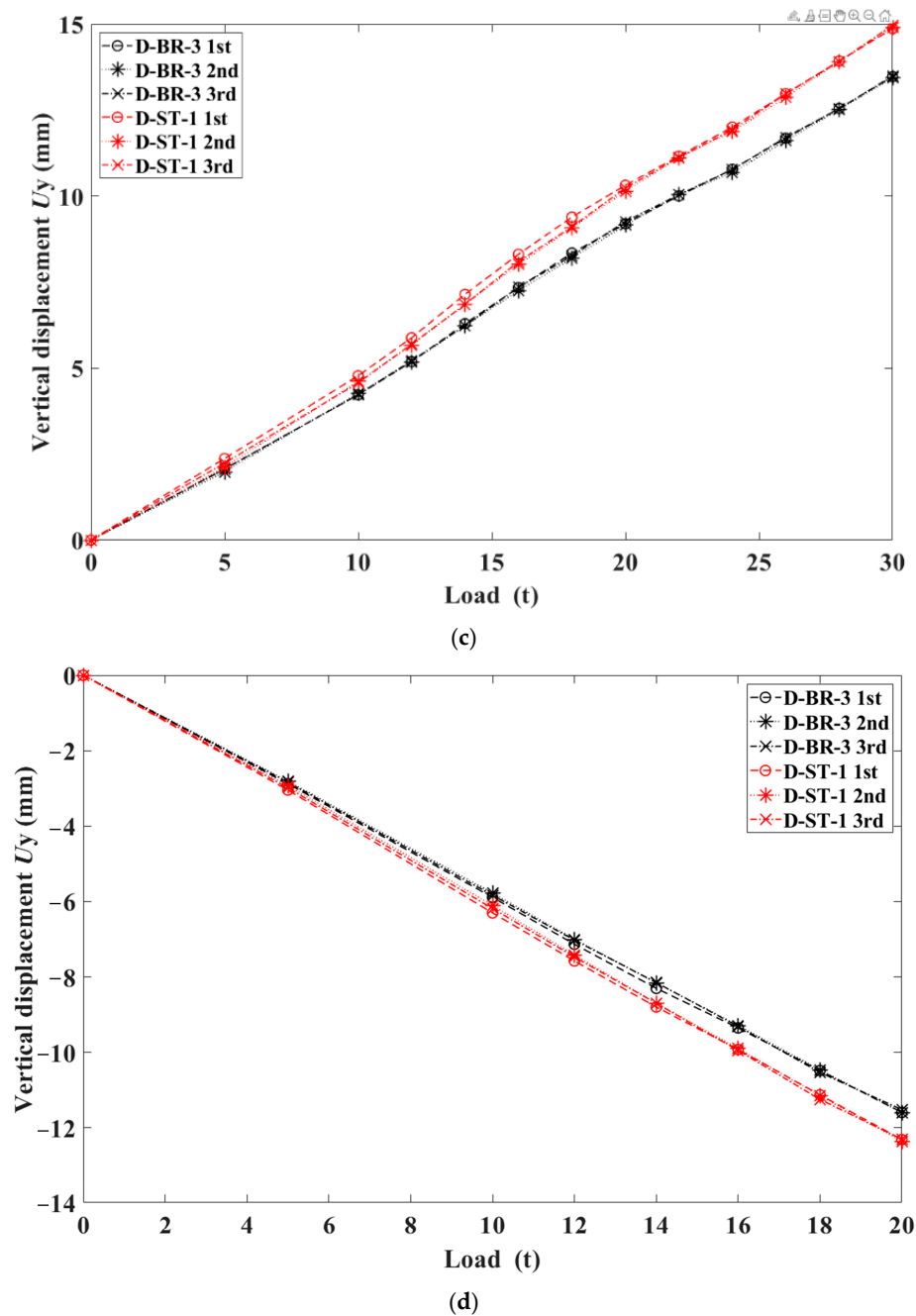


(a)



(b)

**Figure 12.** *Cont.*

(c)



(d)

**Figure 12.** Comparison of multiple measurements of D-BR-3 and D-ST-1 under different working conditions. (**a**) Results of condition 1; (**b**) results of condition 2; (**c**) results of condition 3; (**d**) results of condition 4.

The rotation values of the B1 and B2 bearings can be derived from the displacement results using Equation (1).

$$Rx = \arctan\frac{Uy_2 - Uy_1}{z_2 - z_1} \tag{1}$$

where $Uy_1$ and $Uy_2$ are the displacement values measured by the front and rear gauges of a bearing, and $z_1$ and $z_2$ are, respectively, the longitudinal coordinates of the two gauges. The bearing rotation angle at bearing B1 is obtained by converting the results of D-BR-3 and D-BR-4, and the shaft rotation angle at bearing B1 is obtained by converting the results of D-ST-1 and D-ST-2. The results of D-BR-5 and D-BR-6 can be used to obtain the rotation angle of the bearing's rear end at B2, and the results of D-BR-9 and D-BR-10 can be used

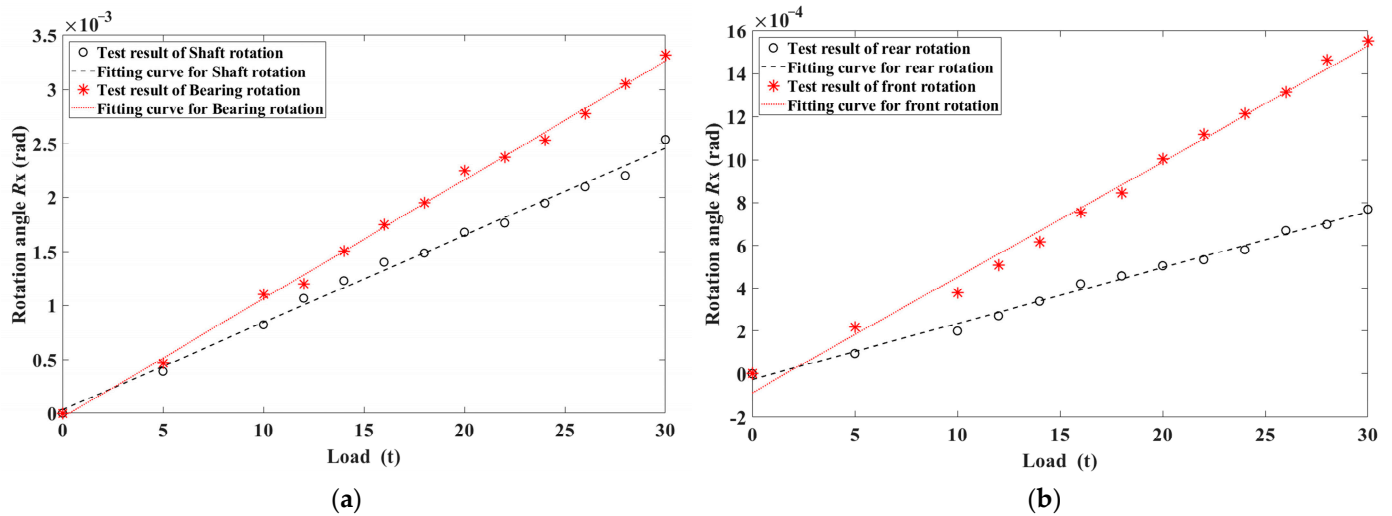to obtain the bearing's front end rotation angle at B2. The rotation results are plotted in Figures 13–16.



**Figure 13.** Comparison of rotation angle results for condition 1. (**a**) Rotation comparison at the B1 bearing; (**b**) rotation comparison at the B2 bearing.
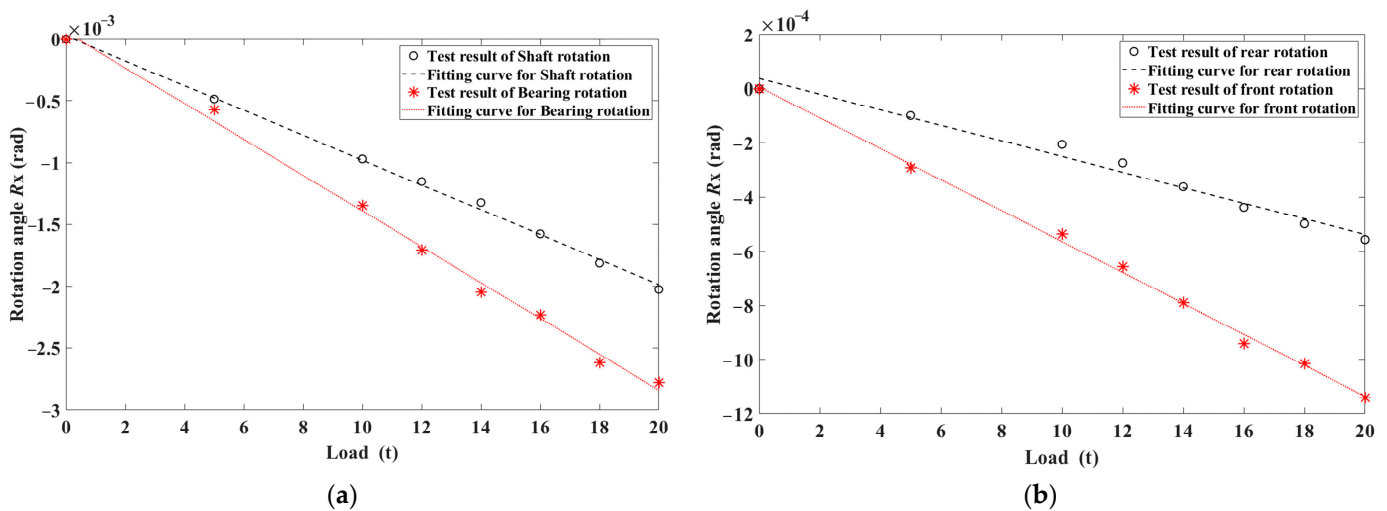


**Figure 14.** Comparison of rotation angle results for condition 2. (**a**) Rotation comparison at the B1 bearing; (**b**) rotation comparison at the B2 bearing.

Figure 13a is a comparison of the results of the rotation angle of the bearing and shaft at B1 under working condition 1, with the dispersed points representing the experimentally determined rotation angles and the two straight lines representing the corresponding first-order fitting curves. Comparing the fitting results to the test results demonstrates that, within the range of hull deformation, the rotation angle of the bearing and the shaft also exhibits a linear change with increasing load. Comparing the bearing and shaft rotation angles reveals that the bearing angle is greater than the shaft angle and that as the load increases, the shaft-to-bearing angle also increases progressively. This indicates that the bearing and shaft rotation angles are affected differentially by hull deformation. This difference obviously modifies the state of action between the shaft and bearing, as will be demonstrated in the pressure results later in this paper.
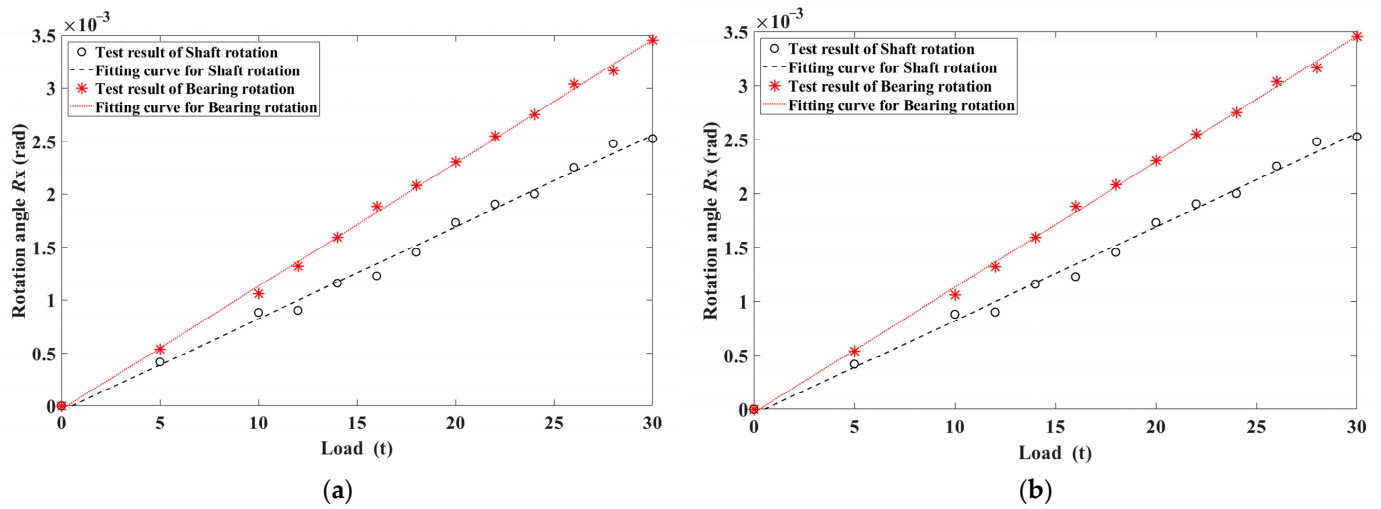
**Figure 15.** Comparison of rotation angle results for condition 3. (**a**) Rotation comparison at the B1 bearing; (**b**) rotation comparison at the B2 bearing.
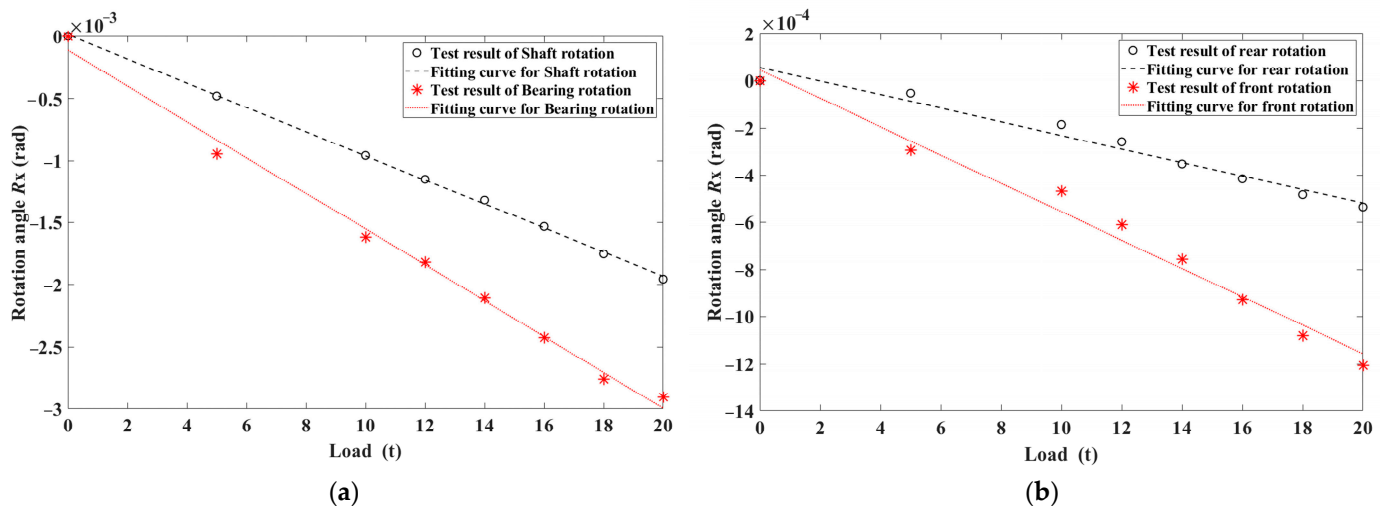


**Figure 16.** Comparison of rotation angle results for condition 4. (**a**) Rotation comparison at the B1 bearing; (**b**) rotation comparison at the B2 bearing.

The variation curves of the rotation angle of the front and rear ends of the B2 bearing under condition 1 are depicted in Figure 13b. Likewise, the curves exhibit a linear change. The rotation angle of the front end of the B2 bearing is always greater than that of the rear end, and the difference progressively increases as the load increases. This law contradicts the conclusion of the cantilever beam theory. In beam theory, the displacement and rotation values are smaller the closer they are to the fixed end. The measured value of the front end has a greater rotational value and is closest to the fixed end because the B2 bearing is the stern tube bearing, located where the presence of the shaft interrupts the longitudinal keel. The rotation angle of the rear end of the B2 bearing is derived from the results of D-BR-5 and D-BR-6, which are located at the top of the stern tube, where the longitudinal keel is free along the *z* axis and cannot bear load. The rotation angle of the front end of the B2 bearing is determined by D-BR-9 and D-BR-10, which are located at the bottom of the stern tube, where the longitudinal keel is connected with the bottom plates and the load can be transferred through the bottom plate; consequently, the rotation value of the lower portion is greater than that of the upper portion. The results of the rotation of the front and rear ends of the B2 bearing indicate that the presence of the stern tube has altered the local structural characteristics, which must be taken into account separately when calculating

the local deformation. When measuring the position and attitude of the stern tube bearing, it is preferable to measure the bearing directly rather than using the measured value of the adjacent area.

Figures 14–16 show the comparison of the results of the rotation angle for condition 2 to condition 4, respectively. The curve change rule is similar to that in Figure 13. Comparing the results of the four working conditions reveals that there is an offset at the fitted curve's beginning point. There are two causes for this error. On the one hand, it is the installation and measurement error of the displacement gauge. Alternatively, it is because the front end of the test body is not fixed rigidly during the test measurement. The front end of the test body is secured by bolts through the shear wall, and a slight rotation of the end face is inevitable under upward and downward loading. This rotation consists of both rigid and elastic components, resulting in variations in the initial points of the fitted curves.

After extracting the slopes of the fitted curves for various conditions, Table 8 can be obtained. It reveals that the slopes of the fitted curves for conditions 1 and 3 are very near to one another, as are the slopes of the fitted curves for conditions 2 and 4. The only distinction between conditions 1 and 3 and between conditions 2 and 4 is the position of the weight suspended on the shaft. Different suspension positions correspond to initial conditions of the shaft that are distinct. When the initial state of the shaft is altered, the rotational law of the bearing and the rotational law of the shaft remain essentially unchanged, indicating that the change trend of the bearing and the shaft in the process of hull deformation is unaffected. This implies, on the one hand, that the initial installation error will always exist in the process of hull deformation. On the other hand, it demonstrates that, when calculating the relative attitude of the bearing and shaft under various hull deformations, the incremental change can be calculated first, followed by the addition of the initial error.

**Table 8.** Comparison of slopes of fitted curves under different conditions.

| Rotation | Slope of the Fitted Curves | | | | | |
|---|---|---|---|---|---|---|
| | Condition 1 ($\times 10^{-5}$ rad/t) | Condition 3 ($\times 10^{-5}$ rad/t) | Relative Error (%) | Condition 2 ($\times 10^{-5}$ rad/t) | Condition 4 ($\times 10^{-5}$ rad/t) | Relative Error (%) |
| Bearing rotation of B1 | 11.01 | 11.64 | 5.65 | −14.41 | −14.49 | 0.56 |
| Shaft rotation of B1 | 8.09 | 8.69 | 7.39 | −9.73 | −10.05 | 3.34 |
| Rear rotation of B2 | 2.61 | 2.40 | −8.19 | −2.87 | −2.88 | 0.24 |
| Front rotation of B2 | 5.39 | 4.97 | −7.69 | −6.01 | −5.71 | −4.95 |

Three bearings' offset values under various conditions have been measured. The bearing reaction force can be calculated based on the offsets using the procedure described in [11]. Table 9 displays the bearing reaction forces. Two reference conditions are added to the table, with reference state 1 being the initial state of conditions 1 and 2, reference state 2 being the initial state of conditions 3 and 4, and the initial loading force being 0 t. As previously indicated, bearing boring is performed after the test hull has been installed on the shear wall, so the initial offset value of each bearing is 0 mm, i.e., the offset value of the bearings in reference state 1 and 2 is 0 mm. However, the initial shaft-to-bearing angle is not zero due to the shaft's deformation caused by gravity. Calculating the initial shaft-to-bearing angles of B2 and B3 in Table 9 is possible. The shaft-to-bearing angles of B2 and B3 cannot be determined owing to the absence of measured shaft rotations.

Comparing the load results of various conditions reveals that the reaction forces of reference state 1 and condition 2 are nearly identical, as are those of reference state 2 and condition 4, but the shaft-to-bearing angle at the B1 position has changed. This indicates that the working state of the bearing has changed, despite the fact that the bearing's reaction force has not altered. When evaluating the working state of bearings, the bearing reaction force alone is insufficient. There is a need for additional parameters, and it is suggested that the shaft-to-bearing angle be added as a supplementary indicator.

*4.2. Bearing Pressure Results*

Based on the bearing B1 pressure test results under various conditions, Figure 17 can be derived. Because the values of the four pressure gauges, P-B1-1, 4, 5, and 8, are always 0 N, they are not displayed. As indicated before, P-B1-1,4,5 and 8 are control groups, arranged on the outside of the contact area. This demonstrates the stability of the measurement system during the measurement. Figure 17a depicts the pressure results for condition 1, and it can be seen that when the load is 0 t, the values of P-B1-6 and 7 at the rear end are greater than the values of P-B1-2 and 3 at the front end. The values of P-B1-6 and 7 increase gradually as the load increases, with the value of P-B1-6 no longer increasing after the load reaches approximately 660 N. This is due to the fact that the measured values have already exceeded the range, and it is therefore impossible to obtain higher values. The values of P-B1-2 and 3 decrease gradually to zero at 18 t and then remain constant, indicating that the shaft and bearing are no longer in contact at this position.

**Table 9.** Comparison of bearing reaction forces of different conditions.

| Condition | Offset (mm) | Shaft-To-Bearing Angle ($\times 10^{-5}$ rad) | Reaction Force (N) | Offset (mm) | Shaft-To-Bearing Angle ($\times 10^{-5}$ rad) | Reaction Force (N) | Offset (mm) | Shaft-To-Bearing Angle ($\times 10^{-5}$ rad) | Reaction Force (N) |
|---|---|---|---|---|---|---|---|---|---|
| | | B1 | | | B2 | | | B3 | |
| Reference state 1 | 0.00 | −7.93 | 3162.1 | 0.00 | 2.25 | 2438.2 | 0.00 | −7.13 | 1051.1 |
| Condition 1 | 12.96 | −85.59 | 3574.4 | 5.96 | / | 1531.2 | 1.37 | / | 1545.8 |
| Condition 2 | −11.35 | 17.06 | 3161.3 | −5.36 | / | 2439.9 | −0.36 | / | 1050.2 |
| Reference state 2 | 0.00 | 15.91 | 2234.9 | 0.00 | −7.23 | 3572.1 | 0.00 | −2.39 | 844.3 |
| Condition 3 | 12.98 | −76.60 | 2672.5 | 5.93 | / | 2609.5 | 1.38 | / | 1369.4 |
| Condition 4 | −11.34 | 28.03 | 2245.6 | −5.36 | / | 3548.5 | −0.34 | / | 857.2 |

Comparing the pressure results with the shaft-to-bearing angle results makes it simple to explain the pressure change pattern. Unloaded, the shaft-to-bearing angle at B1 is $-7.93 \times 10^{-5}$ rad, indicating that the shaft at B1 is aft trim relative to the bearing and that the pressure at the rear end is greater than the pressure at the front end. And as the load increases, the shaft-to-bearing angle progressively becomes $-85.59 \times 10^{-5}$ rad, indicating that the aft trim inclination of the shaft is gradually increased, resulting in an increase in pressure at the stern and a decrease in pressure at the head.

Figure 17b corresponds to condition 2, where the loading direction is the opposite of condition 1, and the values of P-B1-6 and 7 decrease gradually as the load increases, whereas the values of P-B1-2 and 3 increase gradually. This corresponds to Table 9, where the shaft-to-bearing angle changes from $-7.93 \times 10^{-5}$ rad to $17.06 \times 10^{-5}$ rad, the shaft at B1 changes from aft trim to forward trim with respect to the bearing, and the pressure at the front end increases whereas the pressure at the rear end decreases.

Figure 17c,d depict the pressure results for condition 3 and 4, respectively. Unloaded, it can be seen that the pressure at the rear is greater than that at the front. This is consistent with the results against reference state 2, where the shaft-to-bearing angle at B1 is $15.91 \times 10^{-5}$ rad and the shaft is trimmed forward relative to the bearing. Under condition 3, as the loading force increases, the shaft progressively shifts from forward trim to aft trim, the pressure at the rear end of the bearing increases, and the pressure at the front end decreases. In condition 4, the forward trim of the shaft worsens, the pressure at the front end rises, and the pressure at the rear end falls.

The pressure change is a direct indicator of the bearing's working state. The bearing reaction forces are consistent with reference state 1 and condition 2, as are reference state 2 and condition 4. Despite the fact that the bearing reaction forces have not changed, the hull has been deformed by external pressures. The internal pressures have also changed, as illustrated in Figure 17b,d. Finally, it is demonstrated that the bearing reaction force alone is insufficient to discern the bearing's working state; an additional parameter is necessary.

Moreover, a comparison between the pressure results and the shaft-to-bearing angle reveals that the two patterns of change are consistent. This indicates that the thin-film pressure gauges can be used to determine the bearing's state by measuring the relative distribution of pressure inside the bearing. Specifically for the installation process of the shaft, the use of pressure gauges to measure will, to a certain extent, be able to quantify the trim angle of the shaft in relation to the bearing, allowing for a more accurate evaluation of the bearing's state and providing a reference for the adjustment of the shaft installation.
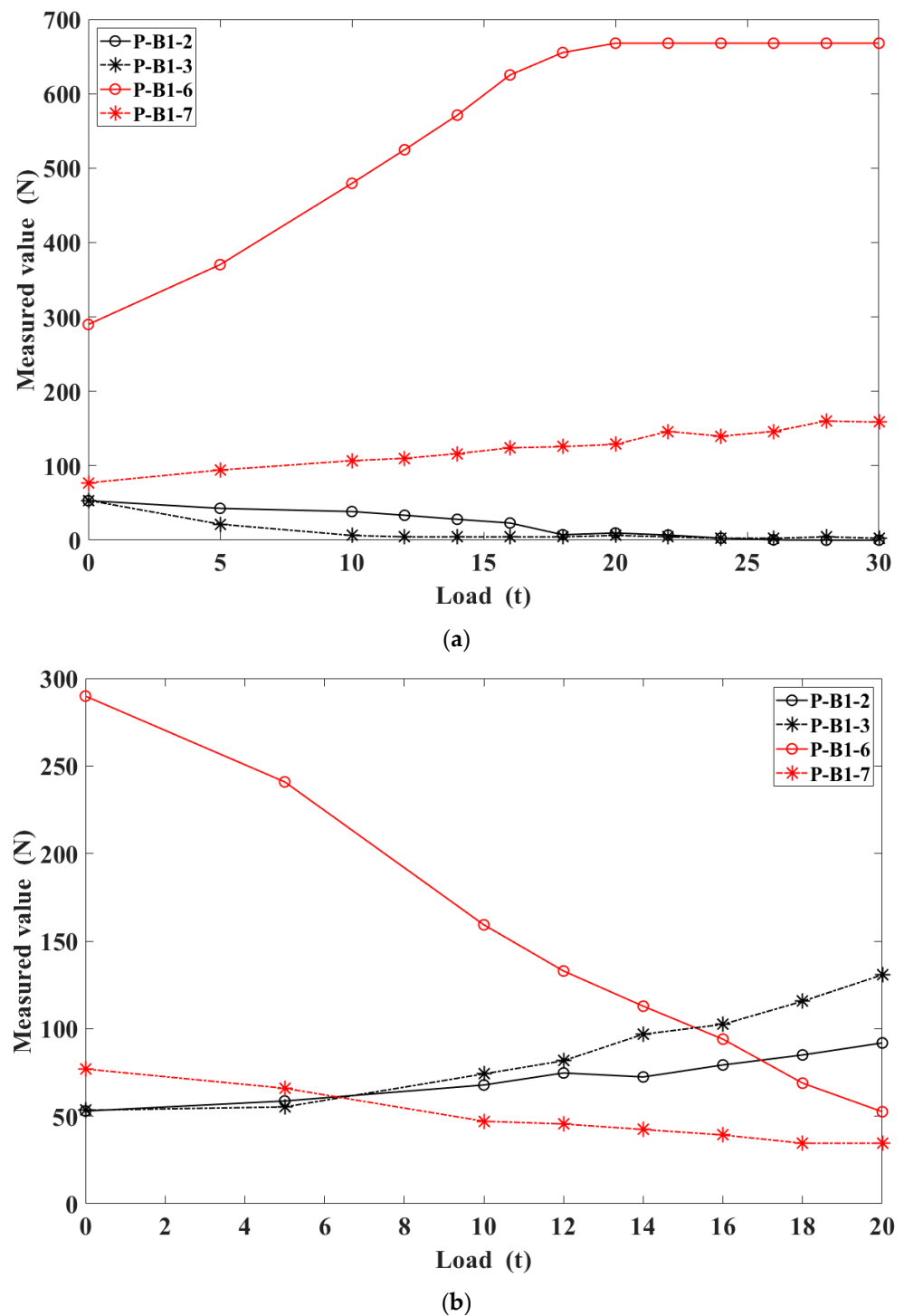


(a)



(b)

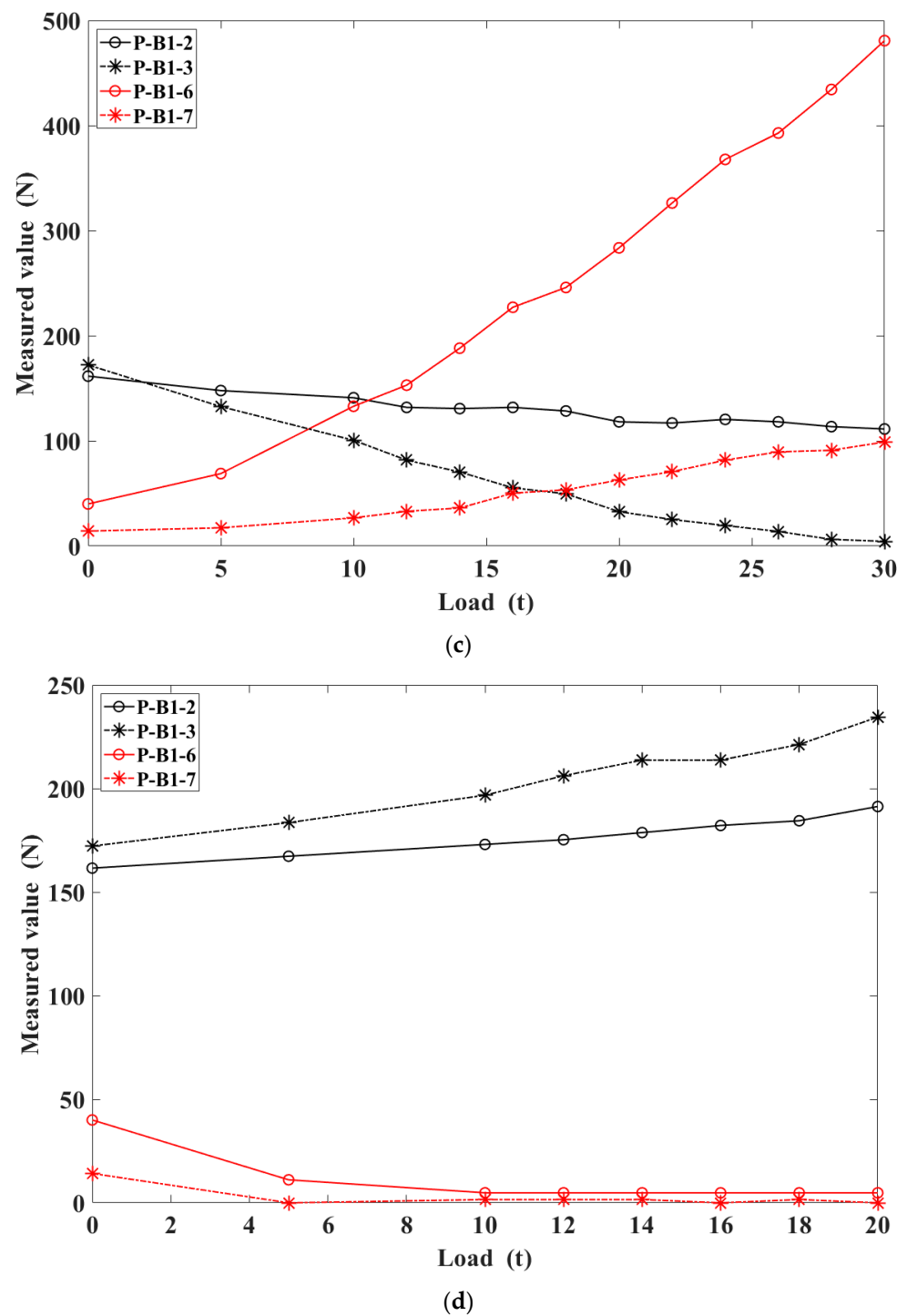**Figure 17.** *Cont.*

(c)



(d)

**Figure 17.** Pressure change curve under different conditions. (**a**) Results of condition 1; (**b**) results of condition 2; (**c**) results of condition 3; (**d**) results of condition 4.

## 5. Conclusions

This paper has presented the design and construction of an integrated hull-bearing-shaft model for a cantilever beam loading test. The displacement gauges monitored the displacement of the bearings and shaft during hull deformation, and a novel type of thin-film pressure gauge monitored the internal pressure distribution of the bearing. The following conclusions can be drawn based on the test results:

1. The linear and reproducible results of multiple displacement measurements for each working condition indicate that the hull deformation was in the elastic stage during the test and that the test results are accurate.

2. As the loading load increases, both the rotation angles of the shaft and bearing increase with analogous magnitudes but distinct slopes. This suggests that the shaft-to-bearing angle change cannot be ignored during hull deformation.

3. The angle of rotation at the stern tube is always greater at the bottom of the forward end than at the top of the aft end because the presence of the stern tube breaks the continuity of the longitudinal keel. In order to acquire accurate values when measuring the rotation angle of the stern tube, it is necessary to measure the bearing as directly as possible. Measuring the rotation of an adjacent structure as opposed to the stern tube may result in a greater error.

4. Different positions of the shaft hanging weights have no effect on the rotation angle change rule of the shaft and bearing, implying that the initial state has nothing to do with the rotation angle change rule of the shaft and bearing during hull deformation.

5. A comparison of bearing load variations reveals that there is a condition in which the hull has been deformed but the bearing reaction force has not changed. Currently, the shaft-to-bearing angle has been altered, and the internal pressure of the bearing has changed consequently, demonstrating that it is insufficient to use the bearing reaction force alone as a criterion for evaluating the bearing's state.

6. Measurement of the internal bearing pressure using thin-film pressure sensors can reflect both the initial tilting of the shaft relative to the bearing as well as the change in shaft-to-bearing angle during hull deformation. This suggests that the use of thin-film pressure gauges to measure bearing pressure can be an effective method for monitoring the state of the bearings during shaft installation.

In future work, the thin-film pressure sensor can be pre-installed within the bearings, allowing the bearing pressure variations to be monitored during both the installation phase and the ship's voyage. The installation pressure data can be used directly to determine the shaft installation's status, and the navigation pressure data can be used to evaluate the bearings' operational status.

**Author Contributions:** Conceptualization, W.Z. and Y.Z.; methodology, W.Z. and Y.Z.; software, W.Z. and Z.R.; validation, W.Z., H.Y. and Z.R.; formal analysis, H.Y.; investigation, W.Z.; resources, H.Y.; data curation, W.Z. and Z.R.; writing—original draft preparation, W.Z.; writing—review and editing, H.Y.; visualization, W.Z.; supervision, H.Y.; project administration, H.Y. All authors have read and agreed to the published version of the manuscript.

**Institutional Review Board Statement:** Not applicable.

**Informed Consent Statement:** Not applicable.

**Data Availability Statement:** Not applicable.

**Conflicts of Interest:** The authors declare no conflict of interest.

# References

1. Avgouleas, K.; Sarris, E.; Gougoulidis, G. Practical Aspects of Propulsion Shaft Alignment, A Virtual Event. In *SNAME International Symposium on Ship Operations, Management and Economics*; SNAME: Pavonia Ave, NJ, USA, 2021.
2. Zhou, R.P. The Theoretic Studies on the Propulsion Shafting Alignment of Ultra-Large Vessels. Ph.D. Thesis, Wuhan University of Technology, Wuhan, China, 2005.
3. Shi, L. Research on Dynamic Alignment of Marine Propulsion Shafting Considering Supporting System Characteristics. Ph.D. Thesis, Dalian University of Technology, Dalian, China, 2010.
4. Mann, G. Analysis of shafting problems using fair curve alignment theory. *Nav. Eng. J.* **1965**, *77*, 117–133. [CrossRef]
5. Mann, G. Shipyard alignment of propulsion shafting using fair curve alignment theory. *Nav. Eng. J.* **1965**, *77*, 651–659. [CrossRef]
6. Piotrowski, J. *Shaft Alignment Handbook*, 3rd ed.;CRC Press: New York, NY, USA, 2006.

7. Marcelo, R.F.; Luiz, A.R.B.; Antônio, C.R.T.; Luiz, A.V.P. Application of the stiffness method to the optimization analysis of a marine propulsion shaft system. *J. Braz. Soc. Mech. Sci. Eng.* **2023**, *45*, 116.

8. Jesse, S.; Hines, J.W.; Edmondson, A. *Motor Shaft Misalignment Bearing Load Analysis*; Citeseer: Gatlinburg, TN, USA, 1999.

9. Jalan, A.K.; Patil, S.; Mittal, G. A Review on Fault Diagnosis of Misaligned Rotor Systems. *Int. J. Perform. Eng.* **2020**, *16*, 499–509. [CrossRef]

10. Li, Z.Y. Research on Shafting Alignment Technology Considering Aft Stern Tube Bearing Incline and Ship Hull Deformation. Master's Thesis, Dalian University of Technology, Dalian, China, 2019.

11. Zhou, W.; Zhao, Y.; Yuan, H.; Wang, X. Study of the Hull Structural Deformation Calculation Using the Matrix Displacement Method and Its Influence on the Shaft Alignment. *J. Mar. Sci. Eng.* **2023**, *11*, 1495. [CrossRef]

12. Lee, J.; Jeong, B.; Tae-Hyun, A. Investigation on effective support point of single stern tube bearing for marine propulsion shaft alignment. *Mar. Struct.* **2019**, *64*, 1–17. [CrossRef]

13. Liao, T.T. Modeling and analysis of laser shaft alignment using 4×4 homogeneous coordinate transformation matrix. *Measurement* **2009**, *42*, 157–163. [CrossRef]

14. Cheng, J.W.; Bu, W.J.; Shi, L.; Fu, J.Q. A real-time shaft alignment monitoring method adapting to ship hull deformation for marine propulsion system. *Mech. Syst. Signal Process.* **2023**, *197*, 110366. [CrossRef]

15. Mankowski, O.; Wang, Q. Real-time Monitoring of Wind Turbine Generator Shaft Alignment Using Laser Measurement. *Procedia CIRP* **2013**, *11*, 291–295. [CrossRef]

16. Lee, J. Application of strain gauge method for investigating influence of ship shaft movement by hydrodynamic propeller forces on shaft alignment. *Measurement* **2018**, *121*, 261–275. [CrossRef]

17. Li, R.; Wang, J.; Chen, Z.Q.; Wang, F.X.; Liu, Y.J. Study on the Methods of Measurement, Optimization and Forecast of Propulsion Shaft Bearing Load of Ships. *J. Mar. Sci. Eng.* **2023**, *11*, 1324. [CrossRef]

18. Yu, Y.F. Research on Dynamic Alignment Method of Ship Propulsion Shafting Considering Hull Deformation. Master's Thesis, Dalian University of Technology, Dalian, China, 2020.

19. Guo, P. The Method of Rational alignment and Load Measurement Technology of Propulsion Shafting. Master's Thesis, Shanghai Jiao Tong University, Shanghai, China, 2020.

20. Yang, H.J.; Zhang, Y.X.; Lu, L.P. Numerical investigation of after stern tube bearing during ship turning maneuver. *J. Mar. Sci. Technol.* **2020**, *25*, 707–717. [CrossRef]

21. Kim, Y.G.; Kim, U.K. Design and analysis of the propulsion shafting system in a ship with single stern tube bearing. *J. Mar. Sci. Technol.* **2020**, *25*, 536–548. [CrossRef]

22. Shi, L.; Xue, D.; Song, X. Research on shafting alignment considering ship hull deformations. *Mar. Struct.* **2010**, *23*, 103–114. [CrossRef]

23. Murawski, L. Shaft line alignment analysis taking ship construction flexibility and deformations into consideration. *Mar. Struct.* **2005**, *18*, 62–84. [CrossRef]

24. Seo, C.; Jeong, B.; Kim, J.; Song, M.; Noh, J.; Lee, J. Determining the influence of ship hull deformations caused by draught change on shaft alignment application using FE analysis. *Ocean Eng.* **2020**, *210*, 107488. [CrossRef]

25. Zhang, S.D.; Long, Z.L.; Yang, X.Y. Reaction force of ship stern bearing in hull large deformation based on stochastic theory. *Int. J. Nav. Archit. Ocean Eng.* **2020**, *12*, 723–732. [CrossRef]

26. Low, K.H.; Lim, S.H. Propulsion shaft alignment method and analysis for surface crafts. *Adv. Eng. Softw.* **2004**, *35*, 45–58. [CrossRef]

27. Ouyang, W.; Zhang, X.B.; Jin, Y.; Yuan, X.Y. Experimental Study on the Dynamic Performance of Water-Lubricated Rubber Bearings with Local Contact. *Shock Vib.* **2018**, *2018*, 6309727. [CrossRef]

28. Ouyang, W.; Cheng, Q.C.; Jin, Y.; Liu, Q.L.; Wang, B.; Wang, L. Lubrication Performance Distribution of Large Aspect Ratio Water-Lubricated Bearings Considering Deformation and Shaft Bending. *Tribol. Trans.* **2021**, *64*, 730–743. [CrossRef]

29. Ouyang, W.; Liu, Q.; Xiao, J.; Huang, J.; Zhang, Z.; Wang, L. Experimental study on the distributed lubrication characteristics of full-size water-lubricated stern bearings under hull deformation. *Ocean Eng.* **2023**, *267*, 2–12. [CrossRef]

30. Zhang, X.; Gu, X. Influence of misalignment angle error on the load-bearing properties of shafting bearing. *Ship Sci. Technol.* **2017**, *39*, 97–102.

31. Sun, J.S.; Kim, Y.G.; Kim, U.K. Study on shaft alignment of propulsion shafting system depending on single reaction force supporting position of aft stern tube bearing. *J. Mar. Sci. Technol.* **2021**, *26*, 1340–1357. [CrossRef]

32. MFF Multi-Point Pressure Test System. Available online: http://www.forcemapping.com/list_3/173.html (accessed on 30 August 2023).